Korean J. Chem. Eng., 35(10), 1979-1987 (2018)
DOI: 10.1007/s11814-018-0108-7

pISSN: 0256-1115
eISSN: 1975-7220

Carbon dioxide reforming of methane over MgO promoted Ni/CNT catalyst

Dehua Zhang, Guangcheng Wei, Yiru Wang, Jing Wang, Ping Ning, Qiulin Zhang†, Mingzhi Wang, Tengfei Zhang, and Kaixian Long

Faculty of Environmental Science and Engineering, Kunming University of Science and Technology, Kunming 650500, P. R. China

(*Received 4 March 2018 • accepted 24 June 2018*)

Abstract−Carbon dioxide reforming of methane to syngas was investigated over a series of MgO promoted Ni/CNT catalysts. MgO played a critical role in improving the catalytic performance of Ni/CNT. The results showed that the addition of MgO strengthened the interaction of Ni and interior surface of CNT. Highly dispersed nickel particles with small size (less than 4.5 nm) were also observed in MgO modified CNT. Otherwise, the NiO nanoparticles were facilely reduced over the catalyst prepared with a narrow size of CNT, as shown in H_2-TPR. The reaction tests demonstrated that the Ni-based catalyst with an addition of MgO and narrow size of CNT exhibited better catalytic activity. Furthermore, the lifetime of Ni-based catalyst was prolonged effectively after adding MgO, attributed to the stabilization and dispersion of Ni particles and the effective restraint on the gasification of CNT.

Keywords: Carbon Dioxide Reforming of Methane, Ni-based Catalyst, Carbon Nanotubes, MgO

INTRODUCTION

With the increasing attention on global warming and energy demand, carbon dioxide reforming of methane (CRM) is becoming a considerable reaction that converts two kinds of plentiful greenhouse gases (CH_4 and CO_2) into syngas [1]. The reaction equation is shown as follows. Hydrogen and carbon monoxide with an optimal ratio (H_2/CO=1 : 1) can be utilized for Fischer-Tropsch synthesis to yield valuable long chain hydrocarbons.

$$CH_4+CO_2 \rightarrow 2CO+2H_2 \quad (1)$$

So far, the promising reaction has not been invested in industrialization. In a comparison of commercial steam reforming of methane (SRM), the problem of CRM is that an adaptive catalyst applied to industrial manufacture is still not found [2,3]. Among the numerous catalysts that have been studied in CRM, nickel-based catalysts are the most popular candidates due to their relative low-cost and extensive availability. However, the deactivation of nickel-based catalyst is inevitable owing to metal sintering and carbon deposition [4-6]. Generally, Ni nanoparticles tend to aggregate at a relatively high temperature and lose catalytic activity. Another knotty issue is that carbon deposition covers the surface of metal particles leading to catalyst deactivation. This fatal problem of CRM occurs when the diameter of active particles grows bigger [7,8]. Previous research has demonstrated that the preparation conditions, the types of additives and the properties of the supports all have influence on the catalytic performance [1]. Hence, finding proper support or promoter is a way to improve the catalytic performance of Ni-based catalysts.

As reported in the previous researches, carbon materials themselves have a certain catalytic ability for carbon dioxide reforming of methane [9-11]. More than that, the carbon materials also play a positive role in preventing extensive amount of carbon deposition from the hydrocarbons [12,13]. Among the various carbon materials, multi-wall carbon nanotubes (MCNT), of which the basic constitution is the layers of graphite, have received considerable attention due to numerous characteristics such as high thermal stability, large surface areas, rich pore structure, confined space and possible modification of electronic properties. Furthermore, MCNT can be manufactured to achieve the desired pore size and used as support to load metals with unique interaction [14]. All these advantages are in favor of improving the catalytic performance [9,15]. Especially, MCNT with tubular morphology has the capability to encapsulate the active metal particles in an ideal size to resist metal agglomeration under high-temperature reaction [16]. Pan et al. [17] reported that the unique electronic structure and defined morphology of MCNT provided an intriguing confinement environment for metal catalysts and catalytic reaction. Up to now, there are limited researches on utilizing carbon nanotubes in the catalysis field of CRM. Qu et al. [18], Ni/Co-SCNT showed excellent performance and thermal stability at 900 °C in the CRM. Ma et al. [19] investigated the different catalytic activity and stability between the catalysts with the nickel nanoparticles inside of CNT and outside of CNT, which showed that Ni particles inside of CNT possessed higher catalytic activity and longer lifetime. Khavarian et al. [20] directly used as-synthesized MCNT as support for CRM and got an approving catalytic performance. At present, Ni/CNT produced by a wet chemical method cannot achieve an unexceptionable conversion rate. And as-synthesized CNT manufactured by catalytic chemical vapor deposition meets a light metal agglomeration and

†To whom correspondence should be addressed.
E-mail: qiulinzhang_kmust@163.com

a quite gasification of CNT occurring during stability test of CRM reaction [21,22]. Therefore, seeking a suitable way to improve the catalytic stability and avoid the loss of support is fundamental for the research and development of Ni supported carbon catalysts.

The surface acid of the support contributes to the formation of carbon deposition; on the contrary, the additional alkaline-earth metals as modification often bring about a positive effect that the coke can be reduced or suppressed. The increased basicity promotes the chemisorption of CO_2 in CRM reaction, which activates CO_2 molecule and augments the concentration of CO_2 on the catalyst, improving the activity of the catalyst [23-25]. Among these alkaline-earth metals, magnesium is widely recognized to apply in CRM on account of its high thermal stability and low cost. To date, the compound of Ni-MgO is an admirable choice to obtain small size Ni particles and alleviate deactivation caused by carbon deposition [26,27]. In many reports, NiO and MgO can form theoretically ideal solid solution to strengthen the metal-support interaction in the system containing Ni and Mg species; however, its formation is dependent on several factors in the preparation process such as calcination temperation, calcination time and Ni content [28]. Jafarbegloo et al. [29] revealed that homogeneous and complete NiO-MgO solid solution was obtained at 600 °C by sufficient interaction between NiO and MgO. Owing to the metal-oxygen bond strength of metal oxide and the metal-metal bond strength of produced solid solution, Ni-MgO solid solution shows higher activity, better resistance to carbon deposition and higher dispersion than other alkaline-earth oxides (such as CaO, SrO, and BaO) in CRM [30]. MgO has a relatively high melting point about 2,850 °C, which endows the capability of high thermal stability on Ni-based catalysts. Moreover, MgO can adsorb CO_2 on the catalyst surface and catalyze the CO_2 reacting with the deposited carbon nearby the metal particles through reverse Boudouard reaction [31].

In this paper, we address the CRM catalytic performance of Ni-based catalysts adding MgO as a promoter. For this purpose, Ni-Mg/CNT and Ni/CNT were prepared by impregnation method. Before the use of CNTs support, it was treated by acid to remove impurities so that the specific surface area, pore volume and adsorption capacity of Ni^{2+} can be improved [25]. Additionally, to determine the effect of pore size, the Ni-based catalysts were synthesized using carbon nanotubes with different pore diameters. All the catalysts were tested in CRM and the physicochemical properties of catalysts were characterized by TEM, N_2 adsorption-desorption, XRD and H_2-TPR.

EXPERIMENTAL

1. Catalyst Preparation

All the raw multiple-wall carbon nanotubes were purchased from Shenzhen Nanometer Gang Co., Ltd, and were classified as narrow pore CNT (np-CNT) and wide pore CNT (wp-CNT), of which pore size was 10-30 nm and 60-100 nm, respectively. Raw MCNT was refluxed in concentrated HNO_3 (68 wt%) at 75 °C for 8 h ultrasonic treatment and washed until pH=7. Then the sample was dried at 100 °C overnight. The first step was aimed at opening up the cap of CNT and cutting CNT into segment. The np-CNT was impregnated with a mixed aqueous solution of $Ni(NO_3)_2{\cdot}6H_2O$ and $Mg(NO_3)_2{\cdot}6H_2O$. The impregnation process should last for 6 h under ultrasonic treatment, and then the sample was stirred to eliminate solvent at room temperature, which benefited to transport particles depositing inside np-CNT. Subsequent samples were dried at 100 °C and calcined at 350 °C in air for 3 h. The proportion of Ni in all catalysts was 5.0 wt%, and the mass loading of MgO was 0 wt%, 1.7 wt%, 5 wt%, 8.3 wt% and 11.7 wt%. Hence, catalysts were named as Ni/np-CNT, Ni-1.7Mg/np-CNT, Ni-5Mg/np-CNT, Ni-8.3Mg/np-CNT and Ni-11.7Mg/np-CNT, respectively. Moreover, in order to study the effect of inner pore size of CNT on the performance of nickel-based catalyst for the CRM, wp-CNT was also used as support to prepare by the same process.

2. Catalyst Characterization

Nitrogen-sorption isotherms of samples were measured at −196 °C using a TriStarII 3020 static volumetric instruments of Micromeritics. The BET surface area and pore size distribution were obtained via Barrett-Emmett-Teller (BET) and Barrett-Joyner-Halender (BJH). Before the measurements, the samples were degassed at 300 °C for 4 h under high vacuum. The crystalline phases of catalysts were examined using X-ray diffraction spectroscopy (XRD, Bruker, D8 Advance) operated with monochromated Cu Kα radiation (operated at 40 kV and 40 mA, λ=0.15406 nm) at room temperature. The particle size and distribution of samples were analyzed by transmission electron microscopy (TEM) (FEI Tecnai G20, 200 kV). Hydrogen temperature-programmed reduction (TPR) was performed in a quartz reactor heated from 100 °C to 800 °C at a heating rate of 8 °C/min with a flowing 5% H_2/Ar gaseous mixture. And the H_2 consumption was monitored by a thermal conductivity detector (TCD) linked to the reactor.

3. Catalytic Reaction

The catalyst was evaluated in a continuous down-flow quartz fixed-bed reactor (i.d.=6 mm) under atmospheric pressure. 50 mg catalyst was compressed and sieved to 40-60 meshes. Prior to the reaction, the catalyst was reduced at 500 °C for 1 h under pure hydrogen (20 ml/min). The reactant gas flow rate to the reactor was set at 30 ml/min, with a gas molar ratio $CH_4 : CO_2 = 1 : 1$. The flow rate (gas hourly space velocity (GHSV)) of the feed was 36,000 ml/h·g_{cat}. The activity of the catalyst was tested from 600 °C to 800 °C at a 50 °C increments. When the temperature increased to the desired value, it was maintained for 30 min before the test. The effluent gases were monitored by an on-line gas chromatograph (Fuli 9790) equipped with a TDX-01 column and a thermal conductivity detector (TCD). The conversions of CO_2, CH_4 and the H_2/CO ratio are defined as follows:

$$\text{Conversion of } CH_4 : X_{CH_4}(\%) = \frac{n_{CH_4,\,in} - n_{CH_4,\,out}}{n_{CH_4,\,in}} \times 100 \tag{2}$$

$$\text{Conversion of } CO_2 : X_{CO_2}(\%) = \frac{n_{CO_2,\,in} - n_{CO_2,\,out}}{n_{CO_2,\,in}} \times 100 \tag{3}$$

$$\text{Selectivity of } H_2(\%) = \frac{n_{H_2,\,out}}{2 \times (n_{CH_4,\,in} - n_{CH_4,\,out})} \times 100 \tag{4}$$

$$\text{Selectivity of CO}(\%) = \frac{n_{CO,\,out}}{[(n_{CH_4,\,in} - n_{CH_4,\,out}) + (n_{CO_2,\,in} - n_{CO_2,\,out})]} \times 100 \tag{5}$$

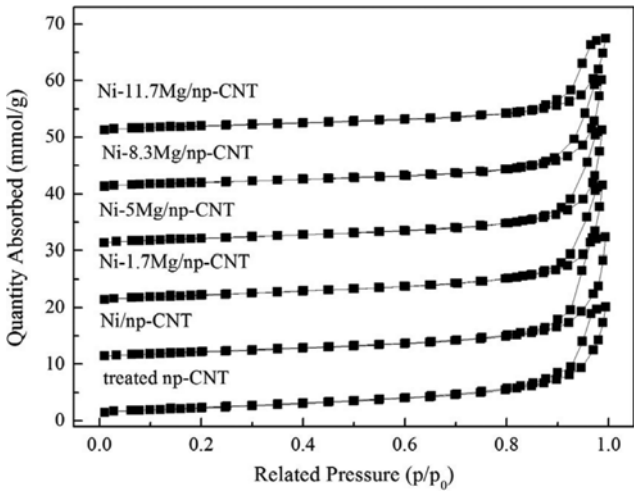

Fig. 1. N_2 adsorption-desorption isotherms of treated np-CNT, fresh Ni/np-CNT and Ni-Mg/np-CNT catalysts.

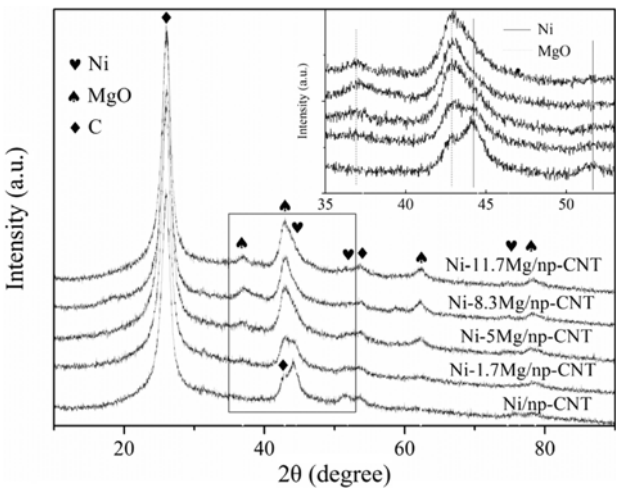

Fig. 2. XRD patterns of reduced Ni/np-CNT and Ni-Mg/np-CNT catalysts.

RESULTS AND DISCUSSION

1. Catalyst Characterizations

1-1. Ni/CNT and Ni-Mg/CNT

The pore structure of samples was analyzed using N_2 adsorption-desorption. The surface area, average pore diameter and pore volume of different catalysts were calculated based on the BJH and BET method. Fig. 1 shows that the type IV isotherm with H1 hysteresis loop was detected on all the samples, indicating that there was capillary condensation in the mesoporous structure. Attributed to a number of accumulated pores, all the adsorption isotherm of samples showed a weak adsorption at low pressures and a sharp increase of adsorption at relatively higher pressures (0.8 p/p_0). Compared with treated np-CNT, the N_2 adsorption quantity of Ni/np-CNT near the p/p_0=1 increased. This could be due to the increase of accumulated pores. As the ratio of loaded MgO augmenting, the N_2 adsorption quantity of catalyst showed a gradual reduction at 1 p/p_0. And an accompanying decline occurred that the surface area cut down from 171.0 m^2/g to 154.9 m^2/g and pore volume decreased from 0.79 cm^3/g to 0.61 cm^3/g in Table 1, suggesting that loaded particles partially filled in the channel of carbon nanotubes [19]. Hence, overloading MgO affected the textural properties of CNT and would further affect the catalytic performance in the catalytic activity test.

Table 1. Textural properties of fresh Ni-Mg/np-CNT catalyst and np-CNT

Sample	Surface area (m^2/g)[a]	Average pore diameter (nm)[b]	Pore volume (cm^3/g)[b]
Treated np-CNT	181.5	15.8	0.72
Ni/np-CNT	171.0	19.5	0.79
Ni-1.7Mg/np-CNT	177.9	19.2	0.76
Ni-5Mg/np-CNT	168.0	21.0	0.75
Ni-8.3Mg/np-CNT	158.3	22.4	0.70
Ni-11.7Mg/np-CNT	154.9	18.8	0.61

[a]Calculated by BET method
[b]Calculated by BJH method

The crystal phase of the samples was analyzed by XRD. In Fig. 2, a strong diffraction peak is located at 2θ=26.2° and a weak diffraction peak is located at 2θ=42.2°, corresponding to the (002) and (100) diffraction patterns of typical graphite layers of CNTs (JCPDS no.75-1621), respectively. It suggests that the CNTs were well graphitized and the intact framework was reserved after HNO_3 treatment [15]. The characteristic peaks identified as 2θ=44.5°, 51.8° and 76.4° were related to (111), (200) and (220) phase of the Ni (JCPDS no. 87-0712). The characteristic reflections of MgO could be found at 2θ=36.9°, 42.9°, 62.3° and 78.6° (JCPDS no. 45-0946). Interestingly, the diffraction peaks of NiO-MgO solid solution were not found, implying the absence of it. The explanation for this could be ascribed to the preparation process of Ni-Mg/npCNT. According to the previous reports, the formation of NiO-MgO solid solution is influenced by many factors during the preparation, among which the calcination temperature is essential to complete incorporation of NiO into the MgO for NiO-MgO solid solution forma-

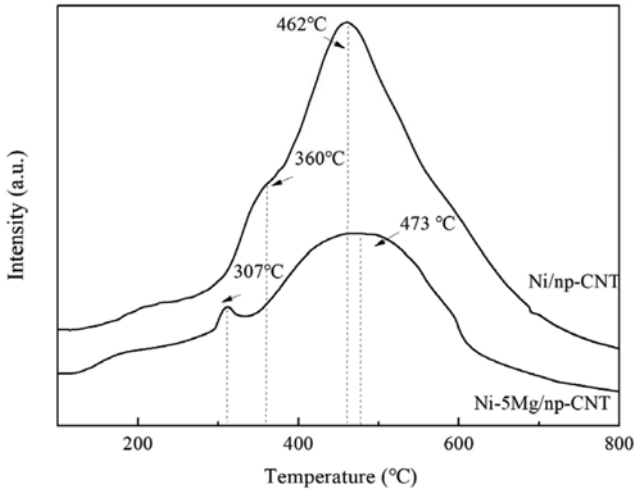

Fig. 3. H_2-TPR profiles of fresh Ni/np-CNT and Ni-Mg/np-CNT catalysts.

tion [32,33]. When the calcination temperature is higher than 400 °C, the NiO-MgO solid solution starts to form and it will complete until at least 600 °C [29]. While, in our work, the calcination temperature was 350 °C. As a result, this kind of species did not form or there was a negligible amount of them in the Ni-Mg/np-CNT catalysts, as confirmed by the XRD patterns.

As shown in the inset of Fig. 2, the diffraction peaks at 2θ= 44.5° and 51.8° corresponding to Ni presented a distinct decline with MgO loading increasing, which indicated the decreasing particle size and improved dispersion. Calculated by the Scherrer equation, the average Ni crystallite diameter was 8.1 nm in Ni/np-CNT and 4.5 nm in Ni-1.7Mg/np-CNT, respectively. While, the diffraction peak of metallic Ni on the other samples was too weak to observed. Thus the diameter of Ni particles was supposed to be highly dispersed and smaller than 4.5 nm. Hence, MgO as a promoter could be an effective way to enhance dispersion of Ni particles and reduce the particle size.

The H_2-TPR was conducted to study the reducibility of the Ni/np-CNT and Ni-Mg/np-CNT and to reveal the changes on the interaction between the active components and support in samples, which was an important factor to impact the catalytic performance. Through analysis of XRD and N_2 adsorption-desorption, Ni-5Mg/np-CNT possessed relatively high surface area and high dispersion of small Ni particles simultaneously. Hence, Ni-5Mg/np-CNT was chosen as the representative for a series of Ni-Mg/np-CNT in the H_2-TPR study. The profile of H_2-TPR was continuous, and two main kinds of NiO species were reduced by H_2 on the broad range of patterns. The first peak at 300-400 °C was associated with the reduction of isolated NiO particles weakly interacting with support. Compared to this peak of Ni/np-CNT, Ni-5Mg/np-CNT possessed the lower reduction temperature with smaller reduction peak area. While, the main reduction peak of Ni-5Mg/np-CNT (473 °C) located at higher temperature and within a wider range than that of Ni/np-CNT (462 °C) did. This phenomenon implied that very small part of isolated NiO particles were more easily reduced, but larger amount of the NiO particles were difficult to reduce due to the strengthened metal-support interaction from adding MgO. Although the NiO-MgO solid solution had higher reduction temperature, as reported by many previous researches [26-29], it was absent here according to the results of XRD. Thus, the main part of active Ni(0) in Ni-5Mg/np-CNT was reduced from Ni(II) species strongly interacting with CNT support, attributing to the effect of MgO promoter [34].

1-2. Ni-5Mg/np-CNT and Ni-5Mg/wp-CNT

Based on the above discussion, we had full cognition about the positive effect of MgO on Ni/CNT catalyst. This section mainly discusses the pore size effect of CNT on the Ni-Mg/CNT catalysts. By comprehensive comparison of serial samples modified with MgO, Ni-5Mg/np-CNT was considered as the best option in all samples. Hence, 5 wt% MgO was selected to prepare the catalyst with different pore sizes of CNT support, and the catalysts were denoted as Ni-5Mg/np-CNT and Ni-5Mg/wp-CNT.

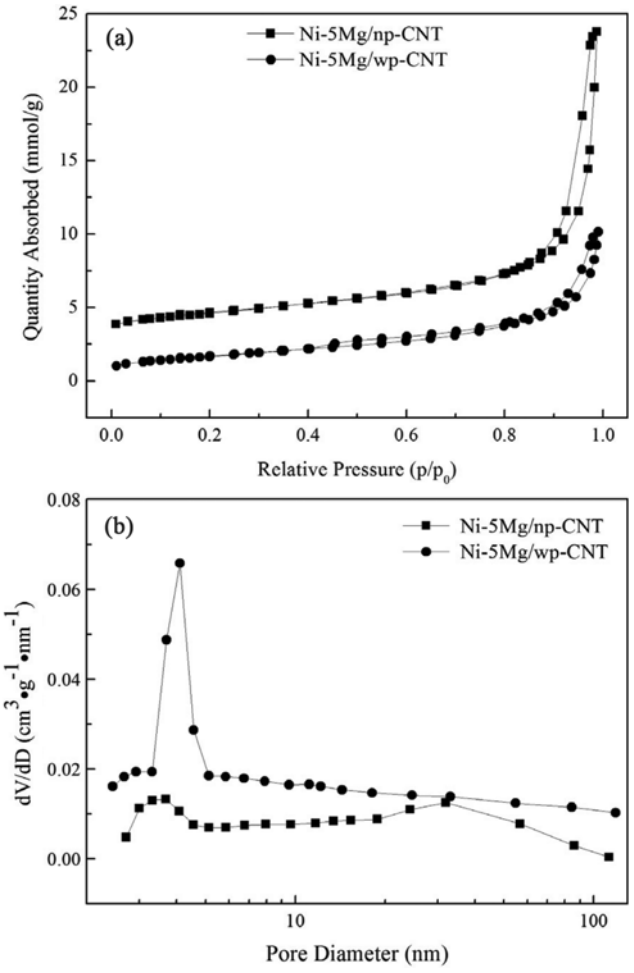

Fig. 4. N_2 adsorption-desorption isotherms and pore distribution of fresh Ni-5Mg/np-CNT and Ni-5Mg/wp-CNT catalysts.

The nitrogen adsorption and desorption isotherms of Ni-Mg/np-CNT and Ni-Mg/wp-CNT are shown in Fig. 4. All the samples had the type IV isotherm with H1 hysteresis loop, which confirmed their mesoporous structure. The quantity of N_2 absorbed on p/p_o=1 decreased as the pore size enlarged, manifesting that Ni-5Mg/np-CNT held more mesoporous and macropores. A similar conclusion was shown in the BET surface area in Table 2. The surface area of Ni-5Mg/np-CNT was larger than that of Ni-5Mg/wp-CNT.

Table 2. Textural properties of fresh Ni-5Mg/np-CNT and Ni-5Mg/wp-CNT catalyst

Sample	Surface area (m^2/g)[a]	Pore volume (cm^3/g)[b]	Average outer diameter (nm)[c]	Average inner diameter (nm)[c]
Ni-5Mg/np-CNT	168.0	0.75	20.5	6.1
Ni-5Mg/wp-CNT	134.4	0.36	57.4	12.8

[a]Calculated by BET method
[b]Calculated by BJH method
[c]Calculated by TEM

The closure point of the N_2 hysteresis loop of Ni-5Mg/wp-CNT was 0.4, and that of Ni-Mg/np-CNT drifted towards high level in 0.8. Therefore, Ni-5Mg/wp-CNT possessed a number of mesoporous. Owing to the different pore size distribution, the pore blockage in Ni-5Mg/np-CNT was acuter than that in Ni-5Mg/wp-CNT. The pore size distribution curves are described in Fig. 4(b). Two visible types of pore represented the inner pore with range from 3.3 nm to 6.7 nm and aggregated pores, respectively [19]. Comparing two samples, narrow pore size of nickel-based catalyst has relatively small mesoporous with range from 2.7 nm to 5.1 nm. As mentioned above, Ni-5Mg/np-CNT suffered a severe reduction of small pores, caused by loaded metal particles blocking inside or end of carbon nanotubes.

The XRD pattern of Ni-5Mg/CNT is shown in Fig. 5. The typical XRD pattern of graphite layers in multi-wall carbon nanotubes was located at 2θ=26.2° and 42.2°. As mentioned before, all the samples kept a complete structure of CNT. Notably, the diffraction peaks at 44.5° and 51.8° corresponding to Ni (111) and Ni (200) had feeble intensity in the catalysts prepared with narrow pore CNT. Whereas, using the CNT support with wide pore size, the characteristic peak of Ni crystallites was obvious, suggesting the wide pore created rich space for crystal lattice growth. Consequently, it could be concluded that the Ni species in Ni-5Mg/np-CNT had higher dispersion and smaller particle size than Ni-5Mg/wp-CNT. Calculated by Scherrer equation, the average Ni crystallite diameter was 3.6 nm in Ni-5Mg/wp-CNT, signifying that the Ni particle size of Ni-5Mg/np-CNT was <3.6 nm.

In Fig. 6, the reducibility of Ni-5Mg/wp-CNT apparently differed from that of Ni-5Mg/np-CNT. In comparison, the reduction peak

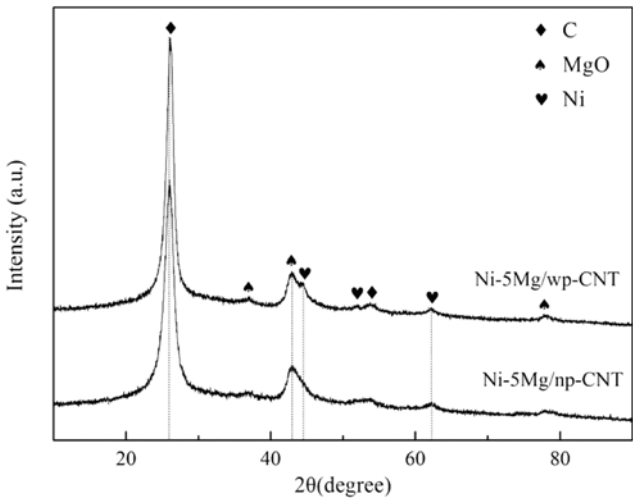

Fig. 5. XRD patterns of reduced Ni-5Mg/np-CNT and Ni-5Mg/wp-CNT catalysts.

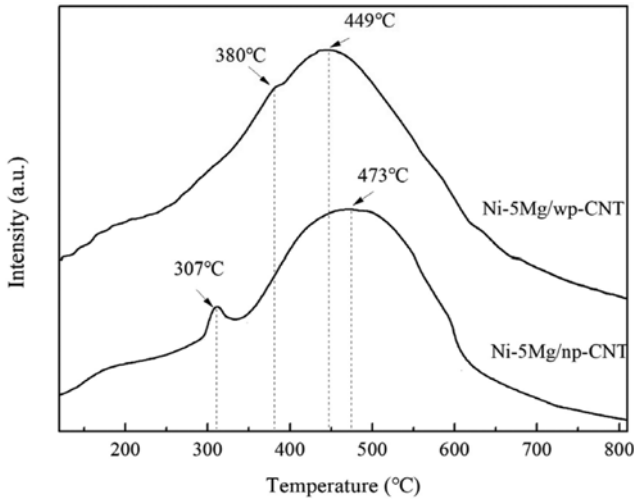

Fig. 6. H_2-TPR profiles of fresh Ni-5Mg/np-CNT and Ni-5Mg/wp-CNT catalysts.

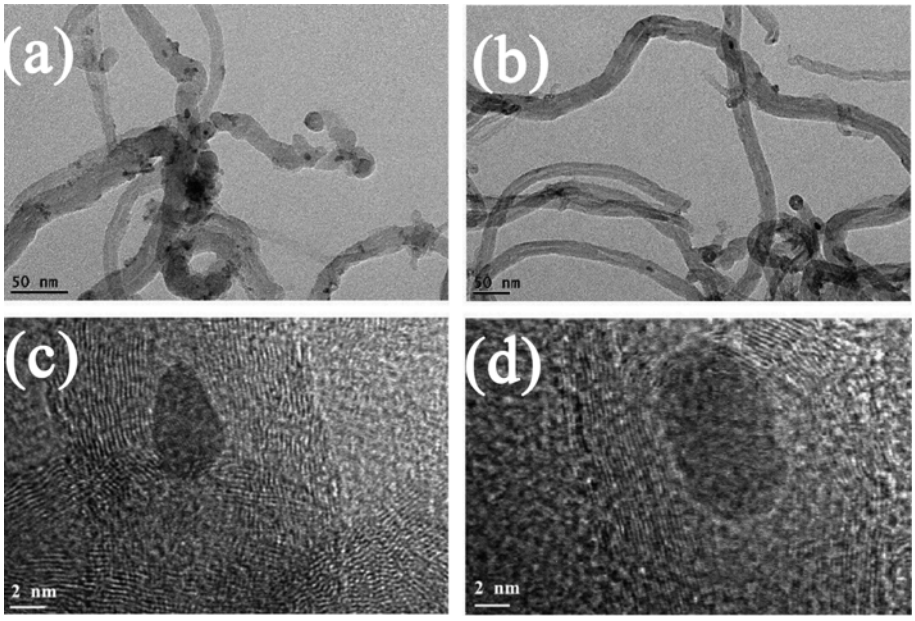

Fig. 7. TEM images of reduced (a), (c) Ni/np-CNT and (b), (d) Ni-5Mg/np-CNT catalysts.

of Ni-5Mg/wp-CNT located at more concentrated temperature range between 350-450 °C than Ni-5Mg/np-CNT. The CNT was endowed with electron-deficient interior surface and an electron-rich exterior surface, which caused by π-electron density shift. The interaction between the π-electron cloud and the metal on the inner wall of carbon nanotubes altered the redox property of the NiO particles [19]. Moreover, the degree on deviation of the graphene layers was different due to various sizes of CNT. As well as the redox properties of Fe and Fe_2O_3 inside of CNT studied by Chen et al., the reduction was dependent on the diameter of CNT channels and facilitated with the diameter decreasing [35]. Consequently, the narrower the tubes, the more facile was the reduction of the confined NiO. Combined with the XRD results, narrow channel space in np-CNT benefited to improve the dispersion of Ni particles and hold the better capability to tunable redox behavior of metal nanoparticles inside CNT.

2. TEM Analysis

Fig. 7(a) displays the morphology of the Ni/np-CNT. Clearly, the majority of CNT end was open after nitrate acid treatment. The nickel particle size was in the range of 4-11 nm, an average about 7.1 nm. The loaded particles of Ni-5Mg/np-CNT detected in Fig. 7(b) could be Ni, MgO or a mixture of them, which were mostly observed in the CNTs. The particle size ranged from 3.7 nm to 10.2 nm, in average about 6.7 nm. While the conclusion on the analysis of XRD indicated that the size of Ni nanoparticles was less than 4.5 nm. In addition, the HR-TEM image clearly verified that there were indeed existing metal particles which deposited inside of CNT in Fig. 7(c), (d). The active metals for CRM were confined by CNT, which largely hampered the particles aggregation under high-temperature reaction.

TEM images of Ni-5Mg/np-CNT and Ni-5Mg/wp-CNT are presented in Fig. 8. Based on the TEM images, the estimated average inner and outer diameter of np-CNT was 6.1 nm and 20.5 nm, respectively. Compared with np-CNT, wp-CNT obviously had wider inner and outer diameter, in average about 12.8 nm and 57.4 nm (Table 2). Due to relatively big pore size, a number of rodlike loaded matters appeared inside tubes of wp-CNT as shown in Fig. 8(b) and Fig. S1. It could be seen that the diameter of Ni particles varied with the size of CNT and confinement effect on the pore size of support significantly impacted the morphology of load [21].

3. Catalytic Activity

The activity of Ni/np-CNT and Ni-Mg/np-CNT was tested in CRM and the conversions are shown in Fig. 9. The activity of all catalysts increased with reaction temperature rising. Adding different weight ratios of MgO boosted the activity for CRM. Obviously, the best activity performance was obtained on Ni-5Mg/np-

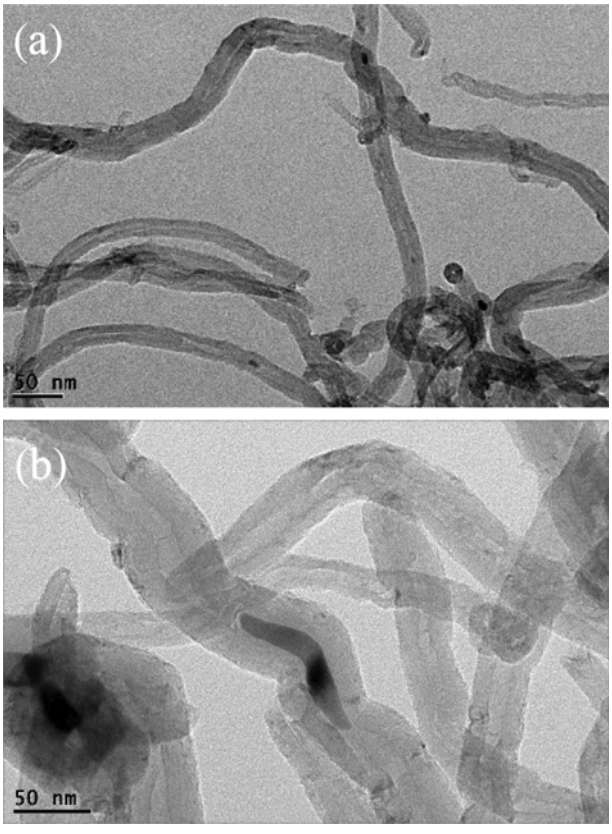

Fig. 8. TEM images of reduced (a) Ni-5Mg/np-CNT and (b) Ni-5Mg/wp-CNT catalysts.

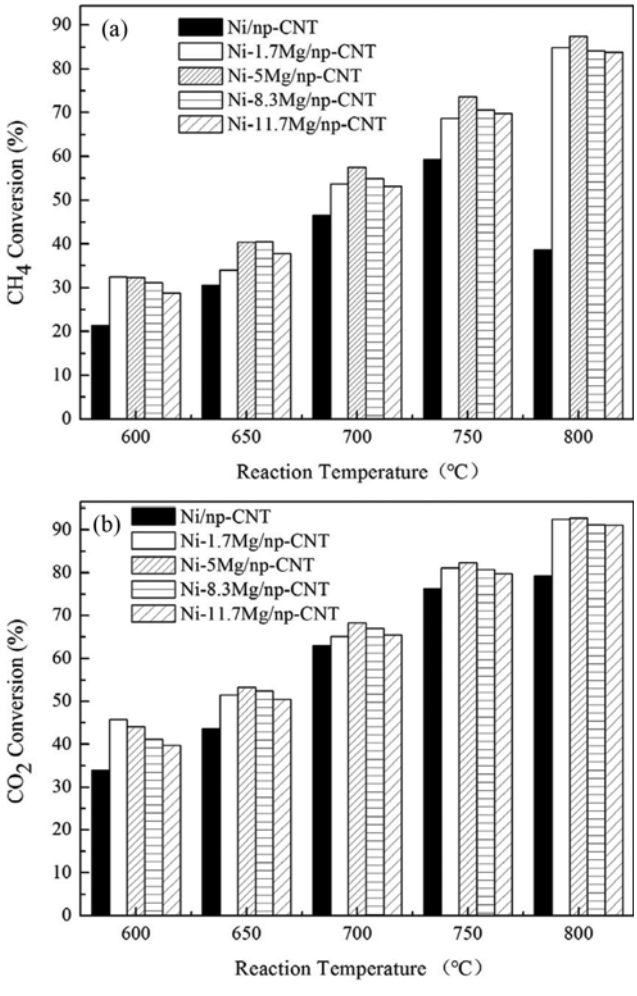

Fig. 9. The conversion-temperature relationships of Ni/np-CNT and Ni-Mg/np-CNT catalyst. (a) CH_4 conversion; (b) CO_2 conversion.

CNT catalyst. Hence we selected it as the representative sample to compare with Ni/np-CNT. Both CH_4 and CO_2 conversions on Ni-Mg/np-CNT were higher than that in Ni/np-CNT, above 12% and 8%, respectively, from 600 °C to 750 °C. Moreover, Ni-5Mg/np-CNT still maintained standout CH_4 conversion around 87% at 800 °C. On the contrary, CH_4 conversion of Ni/np-CNT declined sharply to 38%, while its CO_2 consumption did not decrease with CH_4 consumption dropping. The main reason for this phenomenon should be attributed to the gasification of CNT with CO_2, leading to the loss of support and then the sintering of metal particles caused by particle growth and coalescence [21]. The catalytic activity results indicated that adding MgO enhanced the catalytic activity and the thermal stability of the catalyst. Some comparisons in catalytic activity with other works are provided in Supporting Information (Table S1).

The activity of Ni-5Mg/np-CNT and Ni-5Mg/wp-CNT catalysts in CRM is shown in Fig. 10. It could be found that the methane conversion positively correlated with the diameter of the carbon nanotubes [36,37]. But as a whole, the Ni-based catalyst with smaller pore size CNT support would get higher CH_4 and CO_2 conversions. The confinement effect was not only expounded by the spatial restriction on active particles created by nanosize channels of CNT, but also related to the particular electronic interaction of the nanoparticles in concave of CNT [38]. First, varying diameter channels of CNT enabled tuning the active particle size [39]. Thus, the pore size had a great limitation on the aggregation of nanoparticles under the reaction condition. Secondly, CNT had different elec-

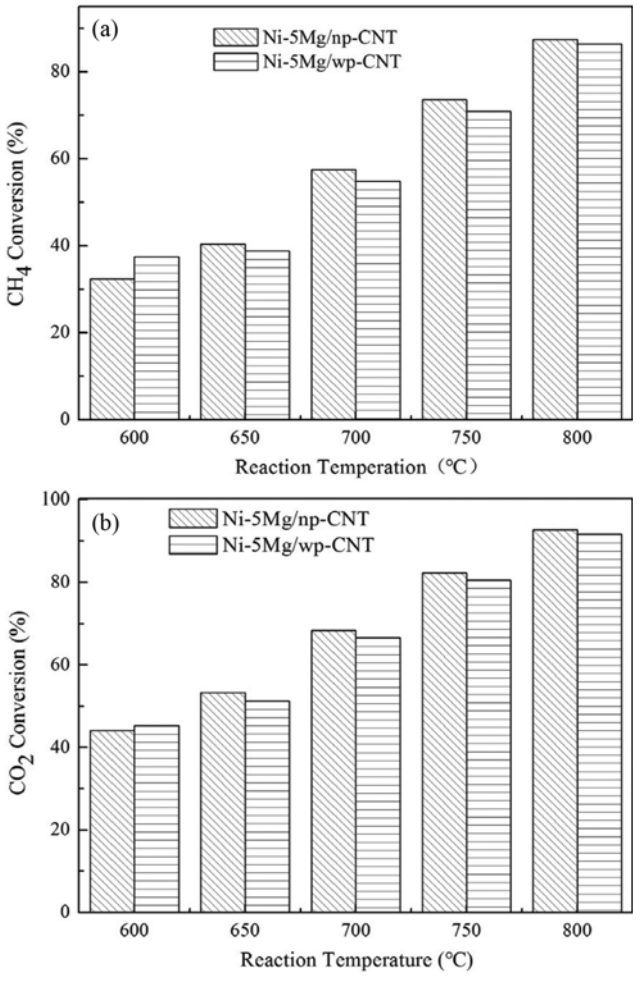

Fig. 10. The conversion-temperature relationships of Ni-5Mg/np-CNT and Ni-Mg/wp-CNT catalyst. (a) CH_4 conversion; (b) CO_2 conversion.

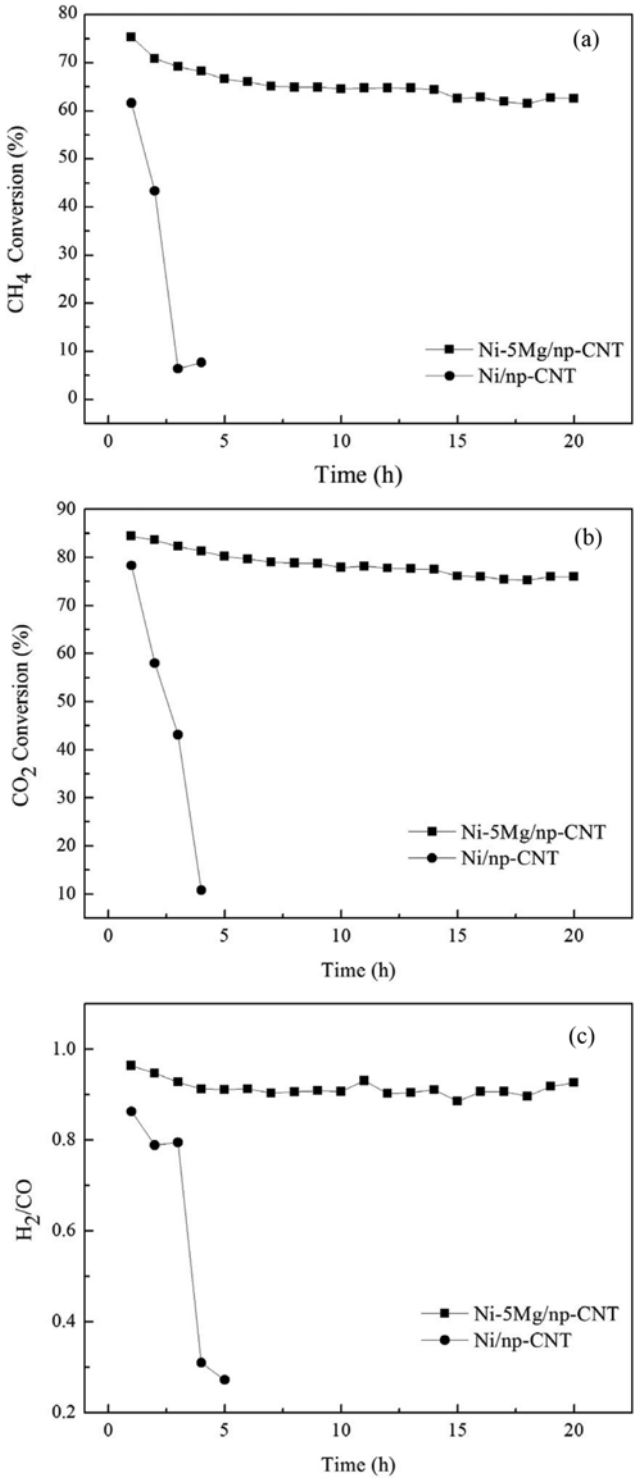

Fig. 11. Catalytic stability of Ni/np-CNT and Ni-5Mg/np-CNT. (a) CH_4 conversion; (b) CO_2 conversion; (c) H_2/CO rat.

tronic properties between the inner and outer surface of the CNT. As the pore size of CNT decreasing, the deviation of graphene layer would be more intense, which contributed to a great distinction of electronic properties. This theory might explain the distinct activity with different pore size CNT supports. This observation did resemble other pore size effect studies in Fischer Tropsch synthesis [36, 37,40]. The carbon balance for all the catalysts is shown in Supporting Information (Fig. S2).

4. Stability test in CRM over Ni/CNT and Ni-Mg/CNT

To evaluate the catalytic stability of Ni-5Mg/np-CNT and Ni/np-CNT, they were conducted at 750 °C for 20 h with a GHSV of 36,000 mL/h·g_{cat} for CRM. As shown in Fig. 11, the CH_4 and CO_2 conversions of Ni/np-CNT declined rapidly, especially in the first four hours. Fortunately, Ni-5Mg/np-CNT exhibited a satisfactory level that the activity decreased slightly with time on stream. After 20 h reaction, CH_4 and CO_2 conversions of Ni-5Mg/np-CNT decreased by 13% and 8%, respectively. Fig. 11(c) shows that the H_2/CO ratio of Ni-5Mg/np-CNT remained between 0.95 and 1.0, suggesting that reverse water gas shift reaction [1] was restrained efficiently. But for Ni/np-CNT catalyst, the CO yield was considerably higher than H_2. This phenomenon hinted that there were several side reactions occurring simultaneously.

Fig. 12(a) shows the morphology of Ni/np-CNT after lifetime test. Owing to a great scale of weight loss, only single multi-wall carbon nanotubes are found in Fig. S3. The sign of breakage also appeared on the tube wall. The Ni particle inside CNT grew up to a rod-like particle with 30.1 nm in length, bigger than the initial size, indicating the growth of metal particles along the nanotubes direction. Therefore, the significant loss of CNT support and the markedly increased particle size accounted for the deactivation of Ni/np-CNT. On the contrary, the metal particle in Ni-5Mg/np-CNT was in length of 22.1 nm after 20 h reaction, but there were still a large number of complete CNT, as shown in Fig. 12(b) and Fig. S4.

Gasification of carbon nanotubes in CRM also appeared in other reports. Mehrnoush et al. [13] held the view that CO_2 would react with unsaturated carbon on carbon nanotubes to produce CO and metal particles took a critical role in activating surface oxygen species and dissociate CO_2 to CO. According to the study of Figueiredo et al. [21], the size of nickel particles was crucially important to control gasification of carbon nanotubes: at any operating temperature; the large Ni particles were easier to remove CNT than the small ones. For Ni-5Mg/np-CNT catalyst, due to the effect of MgO, its active metal Ni presented relatively smaller size than Ni/np-CNT, which was beneficial to control the gasification of CNT. At the same time, the addition of the basic promoter MgO increased the CO_2 absorption, further inhibiting the gasification of CNT support. Furthermore, the Ni species in Ni-5Mg/np-CNT were relatively more stable owing to the strengthened interaction with support by MgO. Hence, Ni-5Mg/np-CNT exhibited superior catalytic performance in CRM than Ni/np-CNT. To sum up, the addition of MgO could enormously lengthen the lifetime of Ni/CNT catalysts and enhance thermal stability by preventing the inherent side reaction from occurrence, which resulted from the reduced Ni metal size, increased CO_2 absorption and improved metal-support interaction.

CONCLUSION

MgO promoted Ni/CNT catalysts were prepared and investigated for carbon dioxide reforming of methane. Highly dispersed nickel species with small particle size were observed after adding MgO. The average size of Ni particles on Ni-Mg/np-CNT samples was less than 4.5 nm. Also, the redox behavior of NiO particles was facilitated within the narrow tube of CNT, implying different interactions between the confined species and CNT surfaces. The addition of 5 wt% MgO effectively prolonged the lifetime of Ni-based catalyst and obtained a stable H_2/CO syngas ratio ranging from 0.95-1.0. The spent Ni/np-CNT sample suffered breakage on the tube wall and weight loss of CNT support, which did not occur on Ni-5Mg/np-CNT. The phenomenon was supposed to be triggered by the gasification of CNT with CO_2, which could be usefully suppressed by small active metal size and improved CO_2 adsorption on MgO. In summary, the addition of MgO as a promoter and selection of narrow tube CNT as support were effective ways to modulate the catalytic performance of CRM.

ACKNOWLEDGEMENTS

This work was supported by National Nature Science Founda-

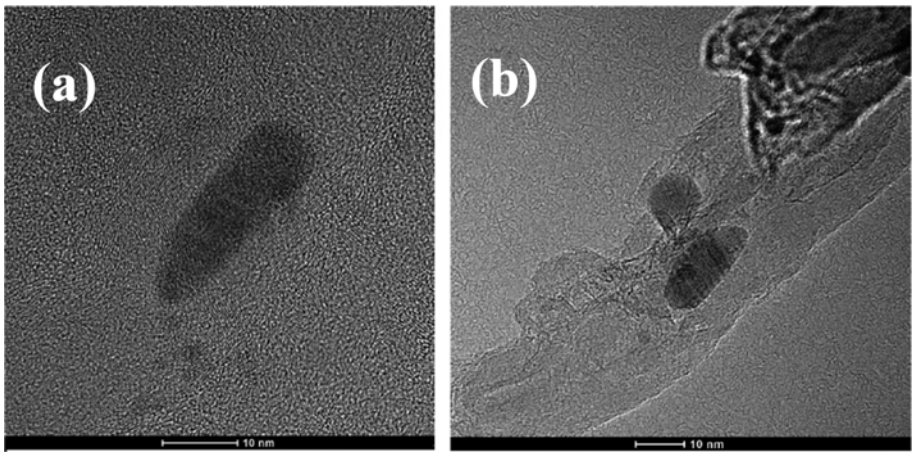

Fig. 12. TEM images of spent (a) Ni/np-CNT and (b) Ni-5Mg/np-CNT catalyst after catalytic stability test.

tion of China (No. 201666014).

SUPPORTING INFORMATION

Additional information as noted in the text. This information is available via the Internet at http://www.springer.com/chemistry/journal/11814.

REFERENCES

1. M. C. J. Bradford and M. A. Vannice, *Catal. Rev. Sci. Eng.*, **41**(1), 1 (1999).
2. V. C. H Kroll, H. M. Swaan and C. Mirodatos, *J. Catal.*, **161**(1), 409 (1996).
3. Y. X. Zeng, L. Wang, C. F. Wu, J. Q. Wang, B. X. Shen and X. Tu, *Appl. Catal., B: Environ.*, **224**, 469 (2018).
4. J. S Choi, K. I. Moon, Y. G. Kim, J. S. Lee, C. H. Kim and D. L. Trimm, *Catal. Lett.*, **52**(1-2), 43 (1998).
5. J. H. Lee, K. Y. Koo, U. H. Jung, J. E. Park and W. L. Yoon, *Korean J. Chem. Eng.*, **33**(11), 3115 (2016).
6. Q. Zhang, J. Wang, P. Ning, T. Zhang, M. Wang, K. Long and J. Huang, *Korean J. Chem. Eng.*, **34**(11), 2823 (2017).
7. W.-J. Jang, H.-M. Kim, J.-O. Shim, S.-Y. Yoo, K.-W. Jeon, H.-S. Na, Y.-L. Lee, D.-W. Jeong, J.-W. Bae, I. W. Nahd and H.-S. Roh, *Green Chem.*, **20**(7), 1621 (2018).
8. E. Akbaria, S. M. Alavi and M. Rezaei, *J. CO_2 Util*, **24**, 128 (2018).
9. G. Zhang, A. Su, Y. Du, J. Qu and Y. Xu, *J. Colloid Interface Sci.*, **433**(11), 149 (2014).
10. Y. Sun, G. Zhang, J. Liu, P. Zhao, P. Hou, Y. Xu and R. Zhang, *Int. J. Hydrogen Energy*, **43**(3), 1497 (2018).
11. G. Zhang, J. Qu, A. Su, Y. Zhang and Y. Xu, *J. Ind. Eng. Chem.*, **21**(1), 311 (2015).
12. G. Zhang, Y. Sun, P. Zhao, Y. Xu, A. T. Su and J. Qu, *J. CO_2 Util*, **20**, 129 (2017).
13. M. Khavarian, S.-P. Chai and A. R. Mohamed, *Fuel*, **158**, 129 (2015).
14. W. Donphai, K. Faungnawakij, M. Chareonpanich and J. Limtrakul, *Appl. Catal., A: Gen.*, **475**, 16 (2014).
15. C. E. Figueira, P. F. M. Junior, R. Giudici, R. M. B. Alves and M. Schmal, *Appl. Catal., A: Gen.*, **550**, 297 (2017).
16. X. Pan and X. Bao, *Chem. Commun.*, **40**(47), 6271 (2008).
17. X. Pan and X. Bao, *Acc. Chem. Res.*, **44**(8), 553 (2011).
18. Y. Qu, A. M. Sutherland and T. Guo, *Energy Fuels*, **22**, 2183 (2008).
19. Q. Ma, W. Ding, M. Wu, T. Zhao, Y. Yoneyama and N. Tsubaki, *Fuel*, **108**(11), 430 (2013).
20. M. Khavarian, S. P. Chai and A. R. Mohamed, *Chem. Eng. J.*, **257**(6), 200 (2014).
21. J. L. Figueiredo, C. A. Bernardo, J. J. C. Jr. and R. T. K. Baker, *J. Catal.*, **110**, 127 (1988).
22. L. M. Esteves, H. A. Oliveira and F. B. Passos, *J. Ind. Eng. Chem.*, (2018), https://doi.org/10.1016/j.jiec.2018.04.012.
23. N. Wang, X. Yu, K. Shen, W. Chu and W. Qian, *Int. J. Hydrogen Energy*, **38**(23), 9718 (2013).
24. Z. Alipour, M. Rezaei and F. Meshkani, *J. Energ. Chem.*, **23**(5), 633 (2014).
25. G. Zhang, P. Zhao, Y. Xua and J. Qu, *J. CO_2 Util*, **18**, 326 (2017).
26. S. M. Lima, J. M. Assaf, M. A. Peña and J. L. G. Fierro, *Appl. Catal., A: Gen.*, **311**(1), 94 (2006).
27. M. Yu, K. Zhu, Z. Liu, H. Xiao, D. Wei and X. Zhou, *Appl. Catal., B: Environ.*, **148-149**, 177 (2014).
28. F. Arena, F. Frusteri, A. Parmaliana, L. Plyasova and N. Shmakov, *Cheminform*, **27**(25), 469 (1996).
29. M. Jafarbegloo, A. Tarlani1, A. W. Mesbah, J. Muzart and S. Sahebdelfar, *Catal. Lett.*, **146**(1), 238 (2016).
30. Y. H. Hu, *Catal. Today*, **148**(3-4), 206 (2009).
31. M. S. Fan, A. Z. Abdullah and S. Bhatia, *Appl. Catal., B: Environ.*, **100**(1-2), 365 (2010).
32. Y. H. Hu and E. Ruckenstein, *Cheminform*, **44**(3), 423 (2002).
33. Y.-H. Wang, H.-M. Liu and B.-Q. Xu, *J. Mol. Catal. A: Chem.*, **299**(1), 44 (2009).
34. F. Pompeo, N. N. Nichio, M. M. V. M. Souza, D. V. Cesar, O. A. Ferretti and M. Schmal, *Appl. Catal., A: Gen.*, **316**(2), 175 (2007).
35. W. Chen, X. Pan and X. Bao, *J. Am. Chem. Soc.*, **129**(23), 7421 (2007).
36. A. Tavasoli, M. Trépanier, A. K. Dalai and N. Abatzoglou, *J. Chem. Eng. Data*, **55**, 2757 (2010).
37. R. M. M. Abbaslou, J. Soltan and A. K. Dalai, *Appl. Catal., A: Gen.*, **379**, 129 (2010).
38. H. Friedrich, S. Guo, P. E. D. Jongh, X. Pan and X. Bao, *ChemSusChem*, **4**(7), 957 (2011).
39. H. Zhang, X. Pan, J. J. Liu, W. Qian , F. Wei , Y. Huang and X. Bao, *International Symposium on Carbon for Catalysis*, **4**(7), 975 (2010).
40. A. Y. Khodakov, A. Griboval-Constant, R. Bechara and V. L. Zholobenko, *J. Catal.*, **206**(2), 230 (2002).